IOP Publishing Journal of Physics A: Mathematical and Theoretical
J. Phys. A: Math. Theor. **50** (2017) 074001 (14pp) doi:10.1088/1751-8121/50/7/074001

Transport in active systems crowded by obstacles

Mu-Jie Huang, Jeremy Schofield and Raymond Kapral[1]

Chemical Physics Theory Group, Department of Chemistry, University of Toronto, Toronto, Ontario M5S 3H6, Canada

E-mail: mjhuang@chem.utoronto.ca, jmschofi@chem.utoronto.ca and rkapral@chem.utoronto.ca

Received 8 July 2016, revised 28 September 2016
Accepted for publication 14 October 2016
Published 12 January 2017

Abstract

The reactive and diffusive dynamics of a single chemically powered Janus motor in a crowded medium of moving but passive obstacles is investigated using molecular simulation. It is found that the reaction rate of the catalytic motor reaction decreases in a crowded medium as the volume fraction of obstacles increases as a result of a reduction in the Smoluchowski diffusion-controlled reaction rate coefficient that contributes to the overall reaction rate. A continuum model is constructed and analyzed to interpret the dependence of the steady-state reaction rate observed in simulations on the volume fraction of obstacles in the system. The steady-state concentration fields of reactant and product are shown to be sensitive to the local structure of obstacles around the Janus motor. It is demonstrated that the active motor exhibits enhanced diffusive motion at long times with a diffusion constant that decreases as the volume fraction of crowding species increases. In addition, the dynamical properties of a passive tracer particle in a system containing many active Janus motors is studied to investigate how an active environment influences the transport of non-active species. The diffusivity of a passive tracer particle in an active medium is found to be enhanced in systems with forward-moving Janus motors due to the cooperative dynamics of these motors.

Keywords: active system, Janus motor, crowded system

(Some figures may appear in colour only in the online journal)

1. Introduction

It is well known that molecular crowding can significantly alter the static and dynamical properties of systems [1–6]. Since the interior of a biological cell is highly crowded by

[1] Author to whom any correspondence should be addressed.

various macromolecular species, numerous studies of the effects of crowding on the structure and transport properties in the cell have been carried out. These investigations have revealed the existence of a wide variety of crowding effects; for example, they have shown that the mean square displacement of particles in the cell often adopts a subdiffusive character on intermediate time scales and that diffusion coefficients may be substantially reduced by crowding. *In vitro* experiments and theoretical studies have also examined the effects of crowding on diffusion and other transport properties, and a substantial literature exists that documents this work [7–11].

Usually the crowding agents are assumed to be passive objects which are subject only to thermal fluctuations due to the environment in which they are immersed. When the crowding agents are themselves active and can move autonomously, one expects and finds that the effects of crowding manifest themselves in different ways. Experiments on passive tracers in suspensions of swimming microorganisms have been carried out and show that the diffusion coefficients of tracers are modified by the flow fields generated by the swimmers [12–14]. Calculations based on hydrodynamic equations have been employed to analyse the effects of these flow fields on tracer dynamics [15, 16]. In an analogous manner, the motions of swimming organisms and particles are altered in systems with passive obstacles, and these altered motions have been studied both experimentally and theoretically [17–19].

In this article we present the results of investigations of reaction and diffusion in two types of system: a diffusiophoretic Janus motor in a suspension of mobile but passive spherical obstacles, and a passive spherical particle in a suspension of chemically powered Janus motors. This investigation has several features that distinguish it from other research on related systems. Our simulations are carried out at a particle-based level that accounts for the chemical dynamics giving rise to many-body concentration fields, hydrodynamics fluid flow and thermal fluctuations. Since the active objects are propelled by a diffusiophoretic mechanism that involves chemical reactions occurring asymmetrically on the motor surface, the reaction rates that are responsible for motion of either the motor in the passive suspension or the active suspension itself are sensitive to the extent of crowding. The chemical gradients that give rise to motor motion are also the dominant factor determining the long range interactions among the motors. Hydrodynamic interactions play a smaller role than for the swimming miroorganisms discussed above, where they provide the major mechanism for the observed collective behavior.

The outline of the paper is as follows: a brief description of the microscopic model for a chemically powered Janus motor immersed in a fluid of reactive particles and obstacles is given in section 2. The active component in the model is based on the asymmetric catalysis of fuel particles into product particles at the surface of the Janus motor and the dynamics conserves the overall mass, momentum and energy of the system while explicitly incorporating the effects of thermal fluctuations and hydrodynamic flow. In section 3, a coarse grain continuum model for the system is presented and the reaction rate for the conversion of fuel into product is derived and compared to simulation results in systems where the motor is crowded by a variable number of passive spherical particles. The structural and dynamical properties of a single Janus motor in the crowded environment are also discussed. In section 4 the effects of an active medium on the dynamics of a passive tracer particle is discussed. The conclusions of the paper are given in section 5.

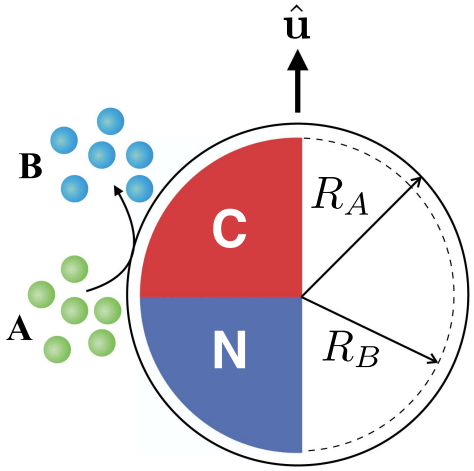

Figure 1. Schematic representation of a forward-moving Janus motor. The motor is composed of catalytic (C) and non-catalytic (N) hemispherical surfaces, where the orientation of the motor is indicated as $\hat{\mathbf{u}}$. The collision radii with solvent particles of type A and B are R_A and R_B, respectively, and the chemical reaction, $A \to B$, takes place on the C surface at radius R_A. In the figure $R_A > R_B$, the motor moves in the $+\hat{\mathbf{u}}$ direction. If $R_A < R_B$, the motor moves backward in the $-\hat{\mathbf{u}}$ direction.

2. Dynamical model

A coarse-grain microscopic description is used to investigate the dynamics of the systems considered in this study. We consider two types of systems: a single active Janus motor in a solution crowded by mobile spherical passive particles, and a passive spherical particle in a solution crowded by active Janus motors. The evolution of the entire system, active Janus motors, passive particles and solvent particles, is carried out by molecular dynamics for solute particles in a binary solvent medium of A and B particles governed by multiparticle collision dynamics [20–23].

The Janus motor is composed of catalytic (C) and non-catalytic (N) hemispheres (see figure 1). Whenever an A particle collides with the catalytic surface of the Janus motor at radius R_A, a chemical reaction converting fuel particles A to product particles B takes place. No reactions occur on the non-catalytic surface of the Janus motor and on the surface of a passive particle. We adopt a hard collision model, discussed in detail elsewhere [24], for the interactions of the solvent particles with Janus motor. Briefly, solvent particles of type $\alpha = A, B$ interact with the Janus motor through hard potentials, $W_{J\alpha}(r) = \infty$ for $r < R_\alpha$, and $W_{J\alpha}(r) = 0$ for $r \geqslant R_\alpha$, where R_α denotes the collision radius. To simplify the notation, we denote the radius R_A by R, the effective radius of the motor. While fuel and product particles may interact with the Janus motors through different potentials, all solvent particles interact with a passive obstacle with the same potential W_P, where $W_P(r) = \infty$ if $r < R$ and $W_P(r) = 0$ if $r \geqslant R$. The solvent particles undergo modified bounce-back collisions at radii R_α for the active Janus motors and at R for the passive spheres, and after a collision the relative velocity between the sphere and the solvent particles is completely reversed. Activity of the Janus motors characterized by directed motion along or away from the director $\hat{\mathbf{u}}$ arises whenever $R_A \neq R_B$, with forward motion along the director occurring when $R_B < R_A$ [24]. In addition to the conversion of A particles into B particles at the catalytic surface of the Janus

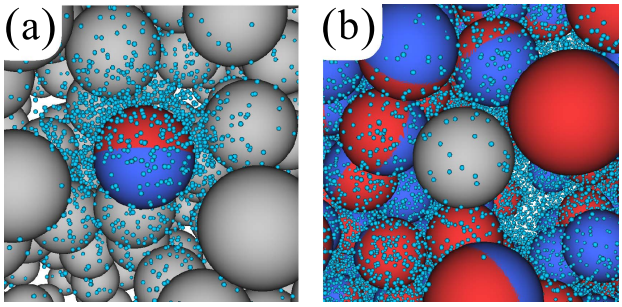

Figure 2. An instantaneous configuration drawn from the simulation of (a) a single Janus motor moving in a passive medium (gray spheres) and of (b) a single passive sphere in an active Janus-motor medium, where the light blue dots are product particles. In panel (b) only $1/10$ of the product particles are shown to aid visualization.

motor, bulk reactions in which B particles are converted back into A particles with rate constant k_2 are incorporated via reactive multiparticle collision dynamic [25]. The bulk reactions allow the establishment of a non-equilibrium steady-state with non-zero concentrations of fuel particles in the system.

While the interactions between solvent particles and solute spherical particles are modeled using hard potentials, any two spheres interact with each other through a soft-repulsive Lennard–Jones potential, $V_{\mathrm{LJ}}(r) = 4\epsilon\,[(\sigma/r)^{12} - (\sigma/r)^6 + 1/4]$, when their distance $r < 2^{1/6}\sigma$, where ϵ is the interaction strength. Further details of the simulation method and the system parameters are provided in the appendix. Results are reported in dimensionless units that are also specified in this appendix.

3. Single motor in a passive, crowded medium

We first consider a single Janus motor operating in a medium with a variable number of N_p passive obstacles (illustrated in figure 2(a)) to investigate how the catalytic rate of reactions occurring at the surface of the Janus particle and the activity of the Janus particle depend on the volume fraction of obstacles in the system.

3.1. Reaction dynamics of a Janus motor

In the usual continuum description for Janus particle motion the chemical concentration fields are described by reaction–diffusion equations and the flow fields by the Stokes equations. Under steady state conditions the velocity of the Janus motor along motor axis $\hat{\mathbf{u}}$ is given by [24, 26–28]

$$V_u = \frac{k_B T}{\eta}\Lambda\langle\hat{\mathbf{u}}\cdot\nabla_{\mathbf{s}}c_B(R,\,\mathbf{s})\rangle_{\mathcal{S}}, \tag{1}$$

where $\mathbf{s}$ denotes coordinates on the surface with radius R, the angle brackets signify a surface average, η is the fluid viscosity and $\Lambda = \frac{1}{2}(R_A^2 - R_B^2)$ for our hard collision model. A knowledge of the product (or fuel) concentration field is needed to compute the Janus motor velocity and the structure of this field is determined by reactions on the Janus motor surface and in the bulk.

To gain insight into the reaction dynamics of the catalytic conversion of A particles to B particles on the surface of the motor, we consider the time evolution of the concentration fields starting from an initial state containing all fuel. Under conditions where the velocity of the motor is small fluid advection is negligible and the time-dependent fuel concentration $c_A(\mathbf{r}, t)$ and product concentrations $c_B(\mathbf{r}, t)$ in a coordinate frame centered on the Janus motor satisfy reaction–diffusion equations,

$$\frac{\partial c_A(\mathbf{r}, t)}{\partial t} = D_0 \nabla^2 c_A(\mathbf{r}, t) + k_2 c_B(\mathbf{r}, t),$$
$$\frac{\partial c_B(\mathbf{r}, t)}{\partial t} = D_0 \nabla^2 c_B(\mathbf{r}, t) - k_2 c_B(\mathbf{r}, t), \tag{2}$$

where D_0 is the common diffusion coefficient for the A and B solvent species. The reaction–diffusion equation must be solved subject to the radiation boundary condition on the Janus motor at a radial distance $r = R$,

$$D_0 \hat{r} \cdot \boldsymbol{\nabla} c_A(r, \theta, t)|_{r=R} = \frac{k_0}{4\pi R^2} c_A(R, \theta, t)\Theta(\theta), \tag{3}$$

where k_0 is an intrinsic rate constant for reaction on the catalytic surface, and $\Theta(\theta)$ is the characteristic function that is unity on the catalytic hemisphere ($0 < \theta < \pi/2$) and zero on the non-catalytic hemisphere ($\pi/2 < \theta < \pi$). In equation (3), the polar angle θ is defined relative to the orientational director axis $\hat{\mathbf{u}}$ (see figure 1). Far from the Janus motor the boundary condition is $\lim_{r\to\infty} c_A(\mathbf{r}, t) = c_0$, where $c_0 = c_A(\mathbf{r}, t) + c_B(\mathbf{r}, t)$ is the total concentration of the A and B species. Using these conditions, we may focus on the solution of the reaction–diffusion equation for $c_B(\mathbf{r}, t)$. It is convenient to Laplace transform the reaction–diffusion equation for the concentration of product, leading to

$$(\nabla^2 - \nu^2)\hat{c}_B(\mathbf{r}, z) = 0, \tag{4}$$

where $\hat{c}_B(\mathbf{r}, z) = \int_0^\infty \mathrm{d}t\ \mathrm{e}^{-zt} c_B(\mathbf{r}, t)$, $c_B(\mathbf{r}, t = 0) = 0$, and $\nu^2(z) = \alpha^2 + \kappa^2$ with $\alpha^2 = z/D_0$ and $\kappa^2 = k_2/D_0$. The solution for the Laplace transform of the concentration of product particles is axisymmetric around $\hat{\mathbf{u}}$ and is given by [24]

$$\hat{c}_B(r, \theta, z) = c_0 \sum_\ell a_\ell(z) f_\ell(r, z) P_\ell(\mu), \tag{5}$$

where $P_\ell(\mu)$ is a Legendre polynomial with $\mu = \cos\theta$, and the radial function $f_\ell(r, z)$ is given by

$$f_\ell(r, z) = \frac{K_{\ell+\frac{1}{2}}(\nu r)}{\sqrt{\nu r}} \frac{\sqrt{\nu R}}{K_{\ell+\frac{1}{2}}(\nu R)}, \tag{6}$$

where $K_{\ell+\frac{1}{2}}(\nu r)$ is a modified Bessel function of the second kind. The coefficients a_ℓ can be determined by solving a set of linear equations and are given by

$$a_\ell(z) = \sum_m (\mathbf{M}^{-1})_{\ell m} E_m, \tag{7}$$

where

$$M_{\ell m} = \frac{2Q_\ell}{2\ell + 1}\delta_{\ell m} + \frac{k_0}{k_D}\int_0^1 \mathrm{d}\mu P_m(\mu) P_\ell(\mu), \tag{8}$$

$$E_m = \frac{k_0}{k_D}\int_0^1 \mathrm{d}\mu P_m(\mu), \tag{9}$$

where $Q_\ell = \nu R K_{\ell+\frac{3}{2}}(\nu R)/K_{\ell+\frac{1}{2}}(\nu R) - \ell$ and $k_D = 4\pi D_0 R$ is the Smoluchowski diffusion-controlled reaction rate coefficient [29, 30]. In the limit $z \to 0$ one recovers the steady state concentration fields discussed earlier [24], and using these solutions the steady state Janus motor velocity is given by $V_u = \frac{k_B T}{\eta}\frac{c_0}{3R}\Lambda a_1$.

We are interested in the net rate of change of the number of product particles $N_B(t)$ in the system at time t and this quantity can be obtained by integrating the time derivative of the product concentration $c_B(\mathbf{r}, t)$ over the volume outside the Janus motor. From equation (2), we find that

$$\begin{aligned}\frac{\mathrm{d}N_B(t)}{\mathrm{d}t} &= D_0\int \mathrm{d}\mathbf{r}\ \delta(r-R)\hat{r}\cdot\boldsymbol{\nabla}c_A(\mathbf{r}, t)\\ &\quad - k_2 N_B(t),\end{aligned} \tag{10}$$

where integration by parts and the fixed sum of concentrations has been used to evaluate the first term on the right. The contribution to the reaction rate due to chemical reactions on the Janus motor surface is $\mathcal{R}_J(t) = D_0\int \mathrm{d}\mathbf{r}\ \delta(r-R)\hat{r}\cdot\boldsymbol{\nabla}c_A(\mathbf{r}, t)$, while $k_2 N_B(t)$ is the contribution to the change in the amount of product due to reactions in the bulk of the solution. Considering the Laplace transform of $\mathcal{R}_J(t)$ and using the solution of the reaction–diffusion equation (5), we obtain

$$\begin{aligned}\hat{\mathcal{R}}_J(z) &= k_D(1+\nu R)a_0(z)c_0\\ &\equiv \hat{k}(z)c_0,\end{aligned} \tag{11}$$

where the last line of this equation defines the z-dependent rate kernel $\hat{k}(z)$ for the reaction on the Janus motor. From equation (11) and the form of $a_0(z)$ one may show that $\lim_{z\to\infty}\hat{k}(z) = k_0/2 \equiv k_J^0$.

In the long time limit the system approaches a steady state, and the corresponding rate coefficient approaches $\hat{k}(z=0) \equiv k_J$. To gain additional insight into the structure of k_J, we may approximate $a_0(z=0)$ by $a_0(z=0) \simeq E_0/M_{00} = k_J^0[k_J^0 + k_D(1+\kappa R)]^{-1}$, so that

$$k_J \simeq \frac{k_J^0 k_D(1+\kappa R)}{k_J^0 + k_D(1+\kappa R)}, \tag{12}$$

which is obtained by neglecting terms $m \neq 0$ in the general expression for $a_0(z)$ in equation (7). This approximate formula has the same structure as that for a spherical catalytic particle with uniform activity in presence of a bulk reaction. It differs in that the value of k_J^0 is half as large as k_0. If the bulk reaction is absent, the result has the same form as that derived earlier by Collins and Kimball [31].

For a single Janus motor, the rate constants can be estimated as $k_J^0 = \sqrt{2k_B T\pi/m}R^2 \simeq 15.7$ and $k_D = 4\pi D_0 R \simeq 2.2$ with $R = 2.5$ and $D_0 = 0.07$, the solvent diffusion constant measured in simulations. In the presence of bulk reaction with reaction rate $k_2 = 0.01$, using equation (12) the steady-state rate coefficient is found to be $k_J \simeq 3.4$, which is somewhat greater than the coefficient $k_J = 2.74 \pm 0.14$ obtained from simulations. Using the full expression for $a_0(z=0)$ one obtains $k_J \simeq 1.97$, which underestimates the rate coefficient. This difference is discussed in the next subsection.

Table 1. Volume fraction dependent intrinsic rate constant $k_J^0(\phi)$, solvent diffusion constant $D_0(\phi)$, and diffusion-controlled rate constant $k_D(\phi)$. The steady-state reaction rate $\mathcal{R}_J$ as a function of volume fraction ϕ obtained from simulations for the active (A) and passive (P) Janus motors and from theoretical estimates (T).

ϕ	0.03	0.061	0.091	0.121	0.151	0.182
$k_J^0(\phi)$	16.38 ± 0.33	16.74 ± 0.64	17.17 ± 0.43	18.02 ± 0.28	18.41 ± 0.37	19.18 ± 0.66
$D_0(\phi)$	0.069	0.068	0.067	0.066	0.065	0.064
$k_D(\phi)$	2.168	2.137	2.111	2.081	2.051	2.025
$\mathcal{R}_J^A(\phi)$	26.9 ± 1.5	26.7 ± 1.4	26.4 ± 1.5	25.8 ± 3.0	25.6 ± 1.5	25.2 ± 1.5
$\mathcal{R}_J^P(\phi)$	24.0 ± 1.3	24.0 ± 1.3	23.8 ± 1.3	23.5 ± 1.3	23.6 ± 1.2	23.5 ± 1.3
$\mathcal{R}_J^T(\phi)$	19.72	19.65	19.59	19.63	19.54	19.53

3.2. Simulation of reaction rate constants

Turning our attention to crowded systems, we consider the rate at which product B particles are produced by the catalytic reaction on the forward-moving Janus motor where $R_B < R_A$. The steady-state reaction rate $\mathcal{R}_J = k_J c_0$ can be computed by counting the total number of fuel particles that enter the surface of the catalytic hemisphere per unit time since all of these particles are converted to product particles in the irreversible reaction on the motor surface. Comparisons of reaction rates can be made between active Janus motors and reactive but passive (non-propelled) Janus spheres where $R_A = R_B = R$ and no propulsion is possible. The results are listed in table 1 for active ($\mathcal{R}_J^A$) and passive ($\mathcal{R}_J^P$) Janus motors in a crowded passive medium for various values of the volume fraction ϕ of obstacles. Although these two reaction rates are within the statistical uncertainty, their means satisfy $\mathcal{R}_J^A > \mathcal{R}_J^P$. For the Janus motor simulations the Péclet number $P_e = V_u(\phi)R/D_0(\phi)$ varies between 0.7 and 1.0 in the ϕ range considered here. Consequently, the solvent concentration fields are slightly perturbed by the directed motion of the motor and this influences the rate of chemical reactions on the motor surface.

In order to compare simulation results with the theoretical expressions for the reaction rate and rate coefficient, we assume that these quantities can be calculated using the development given above in the absence of obstacles but that $k_J^0(\phi)$ and $k_D(\phi)$ depend on the obstacle volume fraction. The rate constant k_J^0 can be determined in simulations from the initial value of the reaction rate for a pure system of fuel particles. For a system containing a single Janus motor, the initial rate k_J^0 can be estimated from the average value of $-(\mathrm{d}N_A(t)/\mathrm{d}t)/c_A(t)$ computed from the first ten MD steps over multiple realizations of the dynamics starting from a pure solvent of fuel particles in the system. In table 1, the rate constant $k_J^0(\phi)$ obtained in this manner for various values of ϕ is listed. The initial rate constant increases with volume fraction, which can be explained by the fact that in a crowded environment fuel particles are confined in the space between obstacles so that initially fuel particles are non-uniformly distributed with an enhancement of fuel particles near the surface of the Janus particle. This enhancement in fuel particle density leads to a higher collision frequency with the catalytic hemisphere of the Janus motor relative to a system without obstacles in which the fuel particles are uniformly distributed [32][2].

[2] In the absence of crowding, the intrinsic rate constant may be estimated using simple kinetic theory as the product of the collision cross section and the mean speed of the fuel particles: $k_J^0 = R_A^2\sqrt{2\pi k_B T/m}$. In crowded systems the collision rate depends on ϕ, so that the rate constant can be approximated as $k_J^0(\phi) = p(\phi)k_J^0$ where the factor $p(\phi)$ accounts for the modification of the collision rate due to crowding. A phenomenological expression $p(\phi)$ can be written as $p(\phi) = 1 + c_1\phi^{c_2}$, where c_1 and c_2 are fitting parameters.

It is well known that crowding can alter solvent diffusion coefficients, so one might expect that the Smoluchowski contribution k_D to the rate coefficient k_J will acquire ϕ dependence through its dependence on the diffusion coefficient, $k_D(\phi) = 4\pi R D_0(\phi)$, where $D_0(\phi)$ is the ϕ-dependent diffusion constant of the solvent in the presence of obstacles.

The volume fraction dependence of the steady-state reaction rate, $\mathcal{R}_J^T(\phi) = k_J(\phi)c_0$, can be computed using these results in the rate coefficient expression, $k_J(\phi) = k_D(\phi)(1 + \kappa(\phi)R)a_0$, with a_0 obtained by solving the full set of linear equations combined with $k_D(\phi)$ and $\kappa(\phi) = \sqrt{k_2/D_0(\phi)}$. The values of $D_0(\phi)$, $k_D(\phi)$ and $\mathcal{R}_J^T(\phi)$ computed from simulations are listed in table 1. Since the expression for $\mathcal{R}_J^T(\phi)$ was derived under the conditions of vanishing Péclet number, it does not depend on the motor velocity and should be compared with simulation results for the passive Janus sphere. The theory underestimates the simulation results. From the form of $\mathcal{R}_J$ above equation (11) we see that it depends on the derivative of the concentration field in the normal direction evaluated on the surface of the Janus sphere. Thus, it is sensitive to the structure of the fields in the boundary layer. Earlier investigations [24] showed that there is a discrepancy between the concentration fields obtained from simulation and continuum theory in the immediate vicinity of the Janus sphere, and this can account for the observed difference in the theoretical predictions and the simulation results.

3.3. Structural and dynamical properties of the crowded active motor system

Structural and dynamical properties of the active motor are also influenced by crowding obstacles in the system. To examine the influence of crowding on the structural properties of the motor system, we consider the distribution of passive obstacles and fuel particles around the motor. The radial distribution function of obstacles around the motor is,

$$g(r) = \left\langle \frac{L^3}{4\pi r^2 N_P} \sum_{i=1}^{N_P} \delta(r_{Ji} - r) \right\rangle, \tag{13}$$

where $r_{Ji} = |\mathbf{r}_J - \mathbf{r}_i|$ is the distance between the center of the Janus motor and ith the obstacle, and $\langle \cdots \rangle$ is the steady-state ensemble and time average over trajectories generated from the molecular dynamics. In figure 3(a), the radial distribution $g(r)$ computed from the simulations in dilute ($\phi = 0.03$, black curve) and dense ($\phi = 0.18$, red dashed curve) media is shown. For a dilute system of obstacles, a sharp peak in the radial distribution function at $r \approx 6$ is evident followed by an uniform distribution of passive obstacles beyond the distance $r \approx 10$, whereas at the higher volume fraction of obstacles the presence of an additional peak at $r \approx 12$ indicates long-range structural ordering of obstacles primarily due to packing effects. As a result of the packed configuration of obstacles, the density of solvent species varies in the radial direction from the Janus motor. The steady-state density of fuel particles around the Janus motor is given by,

$$n_{JA}(r) = \left\langle \frac{1}{4\pi r^2} \sum_{i=1}^{N_A(t)} \delta(r_{Ji} - r) \right\rangle \tag{14}$$

where $N_A(t)$ is the instantaneous number of fuel particles in the system, and $r_{Ji} = |\mathbf{r}_J - \mathbf{r}_i|$ is the distance between the motor and the ith fuel particle. In figure 3(b), we see that the density of fuel particles for a dilute system (black curve) is lowest near the surface of the Janus motor at $r \simeq R = 2.5$ where the catalytic reactions occurs, and monotonically increases to the asymptotic value $c_0(1 - \phi)$. However, as the volume fraction increases, obstacles form a

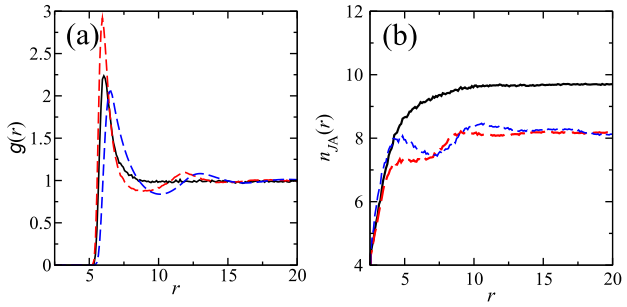

Figure 3. (a) The radial distribution function, $g(r)$, between the active Janus motor and the surrounding passive obstacles and (b) the average density of the fuel particles as a function of distance from the center of the active Janus motor in a dilute ($\phi = 0.03$, black solid curve) and a dense ($\phi = 0.18$, red dashed curve) passive medium. The blue dashed curves in (a) and (b) are for a passive Janus sphere in the dense medium.

packed configuration, and fuel particles are depleted at the position occupied by the obstacles located around $r = 6$.

In addition, motor dynamics affects the structural properties of the surrounding obstacles and fuel particles. This is evident in the plots of $g(r)$ and $n_{JA}(r)$ for a passive Janus sphere, indicated by the blue dashed curves in figure 3. In panel (a), comparing the active and passive Janus particles, the position of the peak for the passive sphere lies at larger separations, indicating a looser structural ordering of the surrounding obstacles. Correspondingly, in panel (b) one sees that the steady-state spherically averaged fuel density in the vicinity of a passive Janus sphere is higher than that for an active motor, indicating a lower steady-state reaction rate as observed in table 1.

Dynamical properties of the Janus motor are also affected by the presence of obstacles. First, we investigate the crowding effects on motor dynamics on different time scales by computing the mean square displacement of the Janus motor, $\Delta r^2(t) = \langle |\mathbf{r}_J(t) - \mathbf{r}_J(0)|^2 \rangle$. In figure 4, the mean square displacement of the motor in a dilute (black circles) and a dense (red squares) system of obstacles is compared. In going from a dilute to a dense crowding medium, the long-time diffusive motions are found to be suppressed, as indicated by the decreasing enhanced diffusion constants with volume fraction listed in table 2. The theoretical expression for the mean square displacement in the absence of obstacles is of the form [33]

$$\Delta r^2(t) = 6D_e t - 2V_u^2 \tau_r^2 (1 - \mathrm{e}^{-t/\tau_r}) - 6\frac{k_B T}{M}\tau_v^2 (1 - \mathrm{e}^{-t/\tau_v}), \tag{15}$$

where V_u is the propulsion speed of the motor along its orientational axis, and τ_v and τ_r are the velocity and motor orientation relaxation times, respectively. In the time regime $\tau_v \ll t \ll \tau_r$, the motor moves ballistically and $\Delta r^2(t) \approx V_u^2 t^2$, whereas when $t \gg \tau_r$, the motion of the motor is diffusive and $\Delta r^2(t) = 6D_e t$. Here the enhanced diffusion constant is given by

$$D_e = D' + \frac{1}{3}V_u^2 \tau_r, \tag{16}$$

where D' is the diffusion constant of a motor without propulsion. To compare the theoretically predicted form of $\Delta r^2(t)$ with simulation results for crowed systems we again assume a similar functional form applies but with parameters that depend on the obstacle

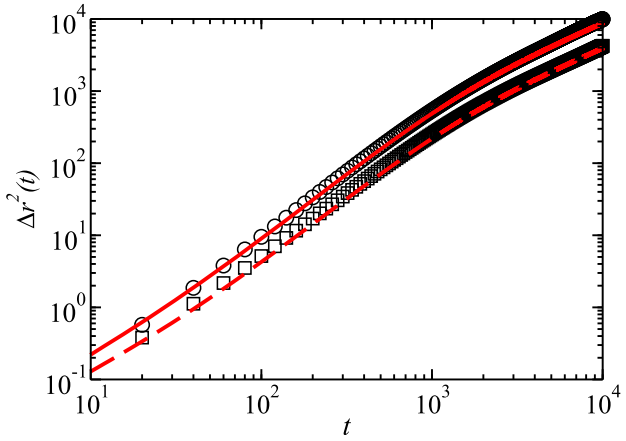

Figure 4. Mean square displacement, $\Delta r^2(t)$, of the active Janus motor in a crowded medium with volume fractions $\phi = 0.03$ (black circles) and $\phi = 0.18$ (black squares). The solid red ($\phi = 0.03$) and dashed red ($\phi = 0.18$) curves are the values of Δr^2 obtained from equation (15) using the values of the transport properties listed in table 2.

volume fraction. Thus, for each ϕ, the simulation values of D', V_u, τ_v and τ_r are required. The diffusion constant D' can be extracted from the $\Delta r^2(t)$ of a passive particle of radius $R = R_A = R_B$ in a crowded system with volume fraction ϕ, and $V_u = \langle \mathbf{V}(\mathbf{t}) \cdot \hat{\mathbf{u}}(t) \rangle$ can be determined by the average of the instantaneous motor velocity $\mathbf{V}(t)$ projected along the motor axis. The velocity relaxation time is $\tau_v(\phi) = D'(\phi) M (k_B T)^{-1} < 2.0$ for all volume fractions considered in this study, and by computing the orientational correlation function of the motor axis from simulation data, $\langle \hat{\mathbf{u}}(t) \cdot \hat{\mathbf{u}}(0) \rangle = \mathrm{e}^{-t/\tau_r}$ and fitting the correlation function with a single exponential, the long-time orientation relaxation time is estimated to be $\tau_r \approx 600$, which is much larger than $\tau_v(\phi)$. The orientational relaxation time is independent of ϕ due to the fact that the interactions between motors are described by central potentials so that no angular momentum exchange occurs in sphere–sphere collisions. Using the simulation values of these quantities (listed in table 2) in equation (16), the predicted mean square displacement of a Janus motor in a dilute ($\phi = 0.03$, red solid curve) and a dense ($\phi = 0.18$, red dashed curve) passive medium are in good agreement with simulation results, as shown in figure 4.

4. A single passive sphere in an active medium

In the previous section the effects of a crowded environment of passive obstacles on a single active motor were investigated. We now consider systems in which the crowding agents themselves are active by embedding a tracer particle in an active medium of Janus motors (see figure 2(b)). It has been shown that a single Janus motor can move in the forward ($+\hat{\mathbf{u}}$) or backward ($-\hat{\mathbf{u}}$) direction depending on the interaction potentials of the Janus particle with the fuel and product particles. The cooperative behavior of collections of forward-moving and backward-moving Janus particles is quite different; for example transient clusters arising from interactions mediated by concentration fields are observed in a collection of forward-moving Janus motors, whereas in a system of backward-moving motors no significant directional and orientational orderings were found [24]. Consequently the collective behavior of these two

Table 2. Volume fraction dependent quantities obtained from simulations, where $V_u(\phi)$ is the propulsion speed along the motor axis $\hat{\mathbf{u}}$, $D_e(\phi)$ is the enhanced diffusion constant of the motor, and $D'(\phi)$ is the diffusion constant of the motor without propulsion.

ϕ	0.03	0.061	0.091	0.121	0.151	0.182
$V_u(\phi)$	0.0276	0.0263	0.0247	0.0227	0.0206	0.0184
$D_e(\phi)$	0.18 ± 0.06	0.17 ± 0.06	0.13 ± 0.03	0.12 ± 0.04	0.10 ± 0.03	0.07 ± 0.02
$D'(\phi)$	0.0030 ± 0.0001	0.0029 ± 0.0001	0.0026 ± 0.0001	0.0024 ± 0.0001	0.0021 ± 0.00005	0.0018 ± 0.00003

Table 3. Volume fraction dependent tracer diffusion constant in an active medium with forward-moving (D^F) and backward-moving (D^B) Janus motors.

ϕ	0.03	0.061	0.091	0.121	0.151	0.182
$D^F(\phi)$	0.0045 ± 0.0015	0.0054 ± 0.0017	0.0064 ± 0.0019	0.0056 ± 0.0025	0.0071 ± 0.0029	0.0068 ± 0.0026
$D^B(\phi)$	0.0040 ± 0.0009	0.0052 ± 0.0020	0.0052 ± 0.0012	0.0050 ± 0.0017	0.0056 ± 0.0019	0.0052 ± 0.0014

active systems and the dynamical effects of the active environment on a passive tracer particle immersed in the active systems are expected to be qualitatively different.

To investigate the influence of active motors on the dynamics of the tracer particle, we compute the mean square displacement of a tracer particle at long times to determine the diffusion coefficients D^F and D^B of the tracer particle in an active medium with forward and backward moving Janus motors, respectively. In the system with forward-moving Janus motors, $D^F(\phi)$ is found to increase with ϕ. Using the data listed in tables 2 and 3, one finds, in going from low ($\phi = 0.03$) to high ($\phi = 0.18$) volume fraction, the ratio $D^F(\phi)/D'(\phi)$ increases from around 1.5 to 4, indicating stronger tracer diffusivity enhancement at high volume fractions. Similar trends are found when the active motors are backward-moving. However, we notice that at low volume fractions ϕ the tracer particle exhibits similar diffusivity regardless the medium properties, whereas at larger ϕ one finds $D^F(\phi) > D^B(\phi)$ indicating stronger interactions between the tracer and the forward-moving motors.

To understand the activity-dependent enhancement of tracer diffusivity, the correlation function $C_{VV}(r)$ between the velocity of the tracer and that of the active motors is computed according to,

$$C_{VV}(r) = \left\langle \sum_{i=1}^{N_f} (\hat{\mathbf{v}}_T \cdot \hat{\mathbf{v}}_i)\delta(r_{Ti} - r) \right\rangle / n(r) \tag{17}$$

where $\hat{\mathbf{v}}_T = \mathbf{v}_T/|\mathbf{v}_T|$ and $\hat{\mathbf{v}}_i = \mathbf{v}_i/|\mathbf{v}_i|$ is the unit vector of the velocity of the tracer particle and of the ith active motor, respectively, and $n(r) = \langle \sum_{i=1}^{N_f} \delta(r_{Ti} - r) \rangle$ is the average number of tracer-motor pairs with separation $r_{Ti} = |\mathbf{r}_T - \mathbf{r}_i|$ at r. In figures 5(a) and (b) the velocity correlation functions $C_{VV}(r)$ in dilute ($\phi = 0.03$) and dense ($\phi = 0.18$) media of forward-moving (black circles) and backward-moving (red squares) motors are shown. From these plots, it is evident that there is no significant correlation at any separation distance between the velocities of the tracer and motor particles at low volume fractions. On the other hand at higher volume fractions, positive correlations in the tracer and motor velocities are observed at both short ($r \simeq 5$) and intermediate separations ($5 < r < 7.5$) for the forward-moving motors, indicating that the tracer is moving along with the motors, whereas a decrease of $C_{VV}(r)$ at small separations is observed for the system with backward-moving motors. In our previous

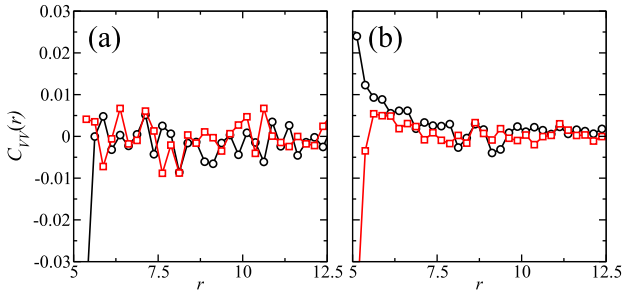

Figure 5. Velocity correlation, $C_{VV}(r)$, between the single passive sphere and the surrounding forward-moving (black circles) or backward-moving (red squares) Janus motors with volume fraction (a) $\phi = 0.03$ and (b) $\phi = 0.18$.

study [24] while no collective motion was seen for a system of backward-moving motors, transient clusters of increasing size with volume fraction were observed in a system of forward-moving Janus motors. The results of $C_{VV}(r)$ and the volume fraction dependent cluster size for forward-moving Janus motors suggest that the passive particle is encapsulated by and moves collectively with forward-moving Janus motors in a dense active medium. This transport enhances the tracer diffusivity, and a larger effective diffusion coefficient is observed in the forward-moving system than that seen in a medium of backward-moving motors.

5. Conclusion

The dynamics and catalytic behavior of a Janus motor in a suspension of passive obstacles was investigated through simulations of a microscopic model. A continuum model for the reaction rate of the conversion of fuel to product particles at the catalytic surface of the Janus motor was constructed and compared in the steady-state regime with the reaction rate observed in simulations. The reaction rate is found to be influenced by the activity of the motor and by the packing structure of surrounding obstacles. The dynamics of the Janus motor was examined from the simulation trajectories and the crossover behavior of the mean square displacement from ballistic to diffusive motion was observed in accordance with theoretical models. The average propulsion speed of the motor and the enhanced diffusion of the motor at long times arising from its activity were found to be suppressed due to crowding. In contrast, the diffusion of a passive tracer was found to be enhanced in a crowded environment of active obstacles, with the strongest enhancements occurring at higher volume fractions. The enhancement of the tracer diffusion was found to be larger in an active medium of forward-moving motors than in backward-moving motors due to the formation of moving transient clusters in the former that carry the tracer particle in a directed fashion.

These observations suggest concentration-mediated interactions among diffusiphoretic Janus motors play an important role not only in their collective behavior but also in their ability to transport material. In particular, our study demonstrates how motor dynamics in a crowded environment can facilitate the transport of passive species such as macromolecules.

Acknowledgments

This work was supported by a grant from the Natural Sciences and Engineering Research Council of Canada. Computations were performed on the GPC supercomputer at the SciNet HPC Consortium. SciNet is funded by: the Canada Foundation for Innovation under the auspices of Compute Canada; the Government of Ontario; Ontario Research Fund—Research Excellence; and the University of Toronto [34].

Appendix. Simulation method and parameters

Simulations are carried out in a periodic cubic box with linear size L. The system contains $N_S = N_A + N_B$ point particles of solvent with N_A fuel and N_B product particles, and the mass of each particle is m. Janus motors and passive particles are modeled as spheres of radius R, volume $V_J = \frac{4}{3}\pi R^3$ and mass $M = V_J c_0 m$ with $c_0 = 10$ the number of solvent particles per unit cubic cell of linear size a, and moment of inertia $I = \frac{2}{5}MR^2$. There are in total $N = N_J + N_p$ solute particles, made up of N_J Janus motors and N_p passive spherical particles, leading to a solute volume fraction of $\phi = (NV_J)/L^3$. The total number of solvent particles in the system is $N_S = c_0(1 - \phi)L^3$. To maintain the system in a non-equilibrium steady state, the reactive multiparticle collision dynamics algorithm is employed [25], where the reaction, $B \xrightarrow{k_2} A$, takes place in the bulk solution with bulk reaction rate $k_2 = 0.01$. Grid-shifting is employed to ensure Galilean invariance [35, 36]. The time evolution of the entire system is carried out using a hybrid MD-MPCD scheme [24].

The results are presented in dimensionless units where mass is in units of m, length in units of a, energies in units of k_BT and time in units of $t_0 = \sqrt{ma^2/k_BT}$. In these units, we have $R = 2.5$, $L = 60$, $M \approx 655$, and $I \approx 1636$. The multiparticle collision time was set to $\tau = 0.1$, with a molecular dynamics step size of $\delta t = 0.01$. The collision radii in the modified bounce back collision with a forward-moving Janus motors are $R_A = 2.5$ and $R_B = 2.4$ and with a backward-moving motor are $R_A = 2.4$ and $R_B = 2.5$, whereas solvent particles interact with passive particles through the same radius $R = 2.5$. The repulsive interaction among spherical has the strength $\epsilon = 1$ and distance $\sigma = 6$.

References

[1] Fulton A B 1982 *Cell* **30** 345
[2] Goodsell D S 1991 *Trends Biochem. Sci.* **16** 203
[3] Zimmerman S P and Minton A P 1993 *Annu. Rev. Biophys. Struct.* **22** 27
[4] Laurent T C 1995 *Biophys. Chem.* **57** 7
[5] Ellis R J 2001 *Trends Biochem. Sci.* **26** 597
[6] Zhou H-X, Rivas G and Minton A P 2008 *Annu. Rev. Biophys.* **37** 375
[7] Metzler R and Klafter J 2000 *Phys. Repts.* **36339** 1
[8] Schnell S and Turner T E 2004 *Biophys. Mol. Bio.* **85** 235
[9] Höfling F and Franosch T 2013 *Rep. Prog. Phys.* **76** 046602
[10] Nakano S, Miyoshi D and Sugimoto N 2014 *Chem. Rev.* **114** 2733
[11] Kuznetsova I M, Turoverov K K and Uversky V N 2014 *Int. J. Mol. Sci.* **15** 23090
[12] Kim M J and Breuer K 2004 *Phys. Fluids* **16** L78
[13] Leptos K C, Guasto J S, Gollub J P, Pesci A I and Goldstein R E 2009 *Phys. Rev. Lett.* **103** 198103
[14] Mino G L, Dunstan J, Rousselet A, Clement E and Soto R 2013 *J. Fluid Mech.* **729** 423
[15] Saintillan D and Shelley M J 2012 *J. R. Soc. Interface* **9** 571
[16] Kasyap T V, Koch D L and Wu M 2014 *Phys. Fluids* **26** 081901

[17] Heddergott N, Krger T, Babu S B, Wei A, Stellamanns E, Uppaluri S, Pfohl T, Stark H and Engstler M 2012 *PLOS Pathogens* **8** e1003023
[18] Berdakin I, Jeyaram Y, Moshchalkov V V, Venken L, Dierckx S, Vanderleyden S J, Silhanek A V, Condat C A and Marconi V I 2013 *Phys. Rev.* E **87** 052702
[19] Soto R and Golestanian R 2014 *Phys. Rev.* E **89** 012706
[20] Malevanets A and Kapral R 1999 *J. Chem. Phys.* **110** 8605
[21] Malevanets A and Kapral R 2000 *J. Chem. Phys.* **112** 72609
[22] Kapral R 2008 *Adv. Chem. Phys.* **140** 89
[23] Gompper G, Ihle T, Kroll D M and Winkler R G 2009 *Adv. Polym. Sci.* **221** 1
[24] Huang M-J, Schofield J and Kapral R 2016 *Soft Matter* **12** 5581
[25] Rohlf K, Fraser S and Kapral R 2008 *Comput. Phys. Commun.* **179** 132
[26] Anderson J L 1983 *Phys. Fluids* **26** 2871
[27] Golestanian R, Liverpool T B and Ajdari A 2007 *New J. Phys.* **9** 126
[28] Kapral R 2013 *J. Chem. Phys.* **138** 020901
[29] von Smoluchowski M 1915 *Ann. Phys.* **48** 1003
[30] von Smoluchowski M 1916 *Phys. Z.* **17** 557
[31] Collins F C and Kimball G E 1949 *J. Colloid Sci.* **4** 425
[32] Echeverria C, Tucci K and Kapral R 2007 *J. Phys.: Condens. Matter* **19** 065146
[33] Colberg P H, Reigh S Y, Robertson B and Kapral R 2014 *Acc. Chem. Res.* **47** 3504
[34] Loken C *et al* 2010 *J. Phys.: Conf. Ser.* **256** 012026
[35] Ihle T and Kroll D M 2001 *Phys. Rev.* E **63** 020201
[36] Ihle T and Kroll D M 2003 *Phys. Rev.* E **67** 066705